



Design of the VLT-CUBES image slicers:

Field re-formatters to provide two spectral resolutions

Ariadna Calcines¹ · Martyn Wells² · Kieran O'Brien¹ · Simon Morris¹ · Walter Seifert³ · Alessio Zanutta⁴ · Chris Evans² · Paolo Di Marcantonio⁵

Received: 10 September 2021 / Accepted: 2 August 2022 / Published online: 5 September 2022
© The Author(s) 2022

Abstract

CUBES is a high efficiency spectrograph designed for a Cassegrain focus of the Very Large Telescope and is expected to be in operation in 2028. It is designed to observe point or compact sources in a spectral range from 300 to 405nm. CUBES will provide two spectral resolving powers: $R \geq 20,000$ for high resolution (HR) and $R \geq 5,000$ for low resolution (LR). This is achieved by using an image slicer for each resolution mode. The image slicers re-format a rectangular on-sky field of view of either 1.5arcsec by 10arcsec (HR) or 6arcsec by 10arcsec (LR) into six side-by-side slitlets which form the spectrograph slit. The slit dimensions are 0.19mm \times 88mm for HR and 0.77mm \times 88mm for LR. The on-sky and physical widths of the slicer mirrors are 0.25arcsec/0.5mm (HR) and 1arcsec/2mm (LR). The image slicers reduce the spectrograph entrance slit etendue and hence the size of the spectrograph optics without associated slit losses. Each of the proposed image slicers consists of two arrays of six spherical mirrors (slicer mirror and camera mirror arrays) which provide a straight entrance slit to the spectrograph with almost diffraction-limited optical quality. This paper presents the description of the image slicers at the end of the Phase A conceptual design, including their optical design and expected performance.

Keywords Image slicer · VLT · UV Spectroscopy · Field re-formatters

✉ Ariadna Calcines
ariadna.calcines@durham.ac.uk

¹ Centre for Advanced Instrumentation, Department of Physics, Durham University, Durham, UK

² UKATC, Royal Observatory, Blackford Hill, EH9 3HJ Edinburgh, UK

³ Landessternwarte, Zentrum für Astronomie der Universität Heidelberg, Königstuhl 12, 69117 Heidelberg, Germany

⁴ INAF - Osservatorio Astronomico di Brera, via E. Bianchi 46, 23807 Merate, LC, Italy

⁵ Osservatorio Astronomico di Trieste, via G. B. Tiepolo 11, 34143 Trieste, Italy

1 Introduction

CUBES (The Cassegrain U-Band Efficient Spectrograph) will be installed on a Cassegrain focus of the VLT to reduce reflection losses in the telescope. Thus, the instrument has to be compact and lightweight. The spectral range extends from 300 to 405nm, providing a significant gain in the combination of sensitivity and spectral resolution in the ground UV compared to existing instruments such as UVES [9] or X-Shooter [10]. The unprecedented efficiency of CUBES at ground ultraviolet (UV) wavelengths will enable a wide range of novel science with the VLT, addressing topics across galactic, extra-galactic and solar system astronomy [1].

Many of the science cases developed for CUBES are presented in detail by other articles in this volume. In brief, the main galactic science cases include the study of stellar nucleosynthesis, both of light elements (e.g. Be) and iron-peak, heavy elements [2] and CNO abundances (e.g. [3–5]). The proposed solar system and planetary science cases focus on the search for water in the asteroid belt and measurements of the N_2/CO ratio in comets. The extra-galactic science cases include measurements of the primordial deuterium abundance, the study of missing baryonic mass in the high-redshift and the origins of the cosmic UV background. The proposed solar system and planetary science cases focus on the search for water in the asteroid belt and measurements of the N_2/CO ratio in comets [6]. The extra-galactic science cases cover the study of missing baryonic mass in the high-redshift circumgalactic medium and the cosmic UV background (e.g. [7]).

A 12-month Phase A conceptual design study of CUBES was completed in June 2021, with a system overview of the Phase A design given elsewhere in this volume [8]. One of the critical elements in the design are the image slicers, which reformat the geometry of the telescope image focal plane into the spectrograph slit. In this article we present the Phase A design of the image slicers, analyse their performance and highlight some of the manufacturing challenges ahead.

2 Specifications

This section presents some of the most relevant specifications for CUBES, as well as those for the design of the two image slicers.

2.1 Specifications for CUBES

The specifications for this instrument are discussed in detail in other articles in this volume. However, the top level requirements with an impact in the image slicers are mentioned in this section and summarised in Table 1.

Table 1 Some of the CUBES Top Level Requirements with an impact in the design of the image slicers

Some of the CUBES Top Level Requirements
High-resolution spectrograph
More than one spectral resolution
Spectral wavelength coverage: 300-405nm
Maximise throughput
No complications or additions should compromise efficiency
Efficiency >40% between 305 and 360nm (goal >45%, with >50% at 313nm)
Efficiency >37% (goal >40%) for the rest of the spectral range

CUBES shall offer more than one spectral resolution. The spectral resolving powers required by the science cases are $R \geq 20,000$ for high resolution (HR) and $R \geq 5,000$ for low resolution (LR). Efficiency is a crucial requirement that should not be compromised by any technical proposal. The required efficiency for its spectral range is:

- >40% between 305 and 360nm (goal >45%, with >50% at 313nm);
- >37% (goal >40%) for the rest of the spectral range.

2.2 Specifications for the image slicers

In order to offer more than one resolution mode, two image slicers are used. The image slicers generate the entrance slit for the spectrograph, whose length shall be sufficient to obtain, in standard seeing conditions, sky spectra up to a distance of at least five times the seeing disk away from the centre of a point-source on both sides of the target. This has resulted in the length of the slices being 10arcsec.

To maximise throughput each image slicer has only two arrays of mirrors: slicer mirror array and camera mirror array. The slicer mirror array is placed at the telescope focus that is re-imaged and magnified by the fore-optics. This allows wider slicer mirrors, reducing manufacturing complexity and costs. The slicer mirror array has six spherical mirrors, each one of them with different tilt angles to reflect a slice of the field towards a camera mirror. In the design for Phase A, all slicer mirrors and all camera mirrors have different radius of curvature. Between the two arrays an intermediate pupil image is generated due to the power of the slicer mirrors. The camera mirrors, also spherical, focus the beams at their focal length. Each camera mirror produces a portion of the spectrograph entrance slit (slitlet) and places the exit pupil at the diffraction grating position. Despite having sliced the field of view, the pupil is recomposed on the grating by the overlapping of all the pupils generated for each slice (see Fig. 6). The width of the slit is different for each resolution mode and so is the field observed in each case. The ratio between the focal lengths of the camera and slicer mirrors provides the magnification required for the defined slit width.

2.2.1 HR image slicer

For the High Resolution (HR) mode, a field of view (FOV) of 1.5arcsec by 10arcsec, corresponding to a linear size of 3mm × 20mm, is decomposed into six slices of 0.25arcsec width by 10arcsec length (0.5mm × 20mm). The image slicer produces a magnification of 0.38, generating the spectrograph entrance slit, whose dimensions are 88mm length by 0.19mm width. The slit is composed of the images of the six slices (called slitlets), whose dimensions are 0.19mm × 7.6mm, plus five gaps of 8.36mm each. The large gaps between slitlets are the result of having only 2 mirrors in the optical path of each slice and for all slices of the field of view to have a common exit pupil (see Fig. 6). It is also the case that because of the need for a detector with 9k pixels in the spectral direction, there is sufficient space to accommodate the overall spectrograph slit length. The slit length has been specified by the spectrograph design as the maximum to achieve good optical quality.

2.2.2 LR image slicer

For the Low Resolution (LR) mode, a field of view of 6arcsec by 10arcsec, corresponding to a linear size of 12mm × 20mm, is decomposed into six slices of 1arcsec width by 10arcsec length (2mm × 20mm). The magnification of the image slicer is the same, 0.38, and the dimensions of the spectrograph entrance slit are 88mm length by 0.77mm width. At the slit position, a field mask is used to define the spectrograph entrance slit. A different mask per resolution mode is required due to the different widths of the slitlets. The specifications for HR and LR modes are shown in Table 2.

3 Interfaces

The image slicers are placed between the fore-optics and the spectrograph. Their location in the end-to-end optical design is presented in Fig. 1.

The VLT Unit Telescopes are 8.20m Ritchey-Chretien reflectors. At their Cassegrain focus, the plate scale is 1.9arcsec/mm and the focal-ratio is F/13.41, with the exit pupil at 14927mm before the focus. The CUBES fore-optics change the

Table 2 Specifications for the design of the image slicers

Parameter	Image Slicer specifications	
	HR	LR
FOV (width x length)	1.5arcsec × 10arcsec (3mm × 20mm)	6arcsec × 10arcsec (12mm × 20mm)
Number of slices	6	6
Slicer mirror width	0.5mm (0.25arcsec)	2mm (1arcsec)
Output slit width	0.19mm	0.77mm

Fig. 1 Location of the image slicers in the CUBES global layout, between the fore-optics (after the telescope focus) and the spectrograph

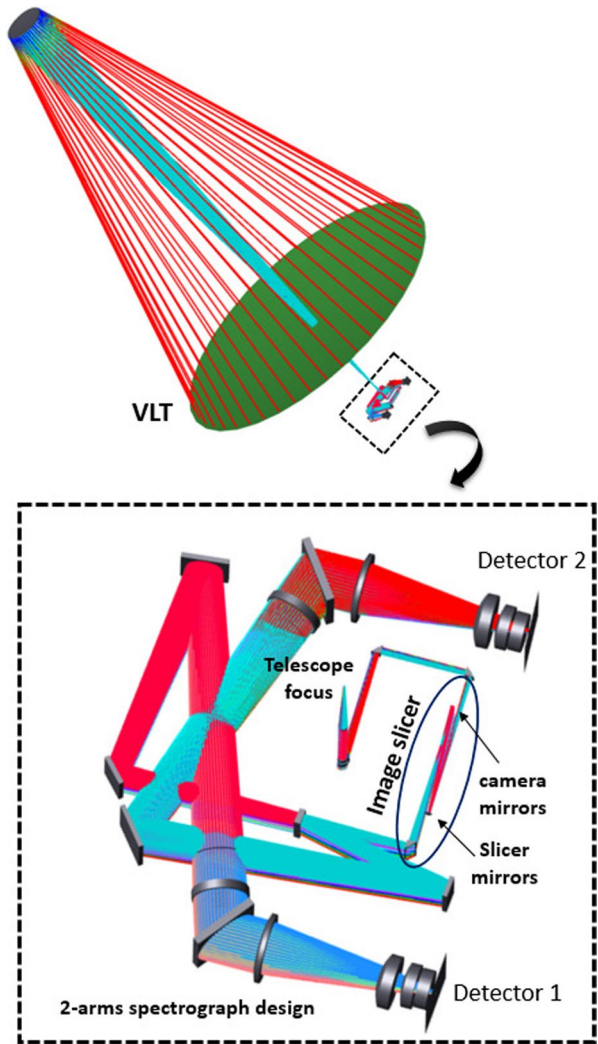


plate scale to 0.5arcsec/mm at the slicer position. It also produces an image of the exit pupil at 1160.39mm before the focus, where the slicer mirror array is placed. The fore-optics are not used only as a reimaging system, they maintain a stable exit image and pupil at a wavelength of 365nm (chosen for calibration purposes using a Hg light source). The fore-optics also provide atmospheric dispersion correction over the whole spectral range for zenith angles between 0 and 60 degrees and, including residual dispersion and other aberrations, the polychromatic image RMS diameter is <0.1arcsec. The overall image quality at the slicer is therefore dominated by the seeing. The fore-optics also provide an interface to an acquisition and guiding camera used to stabilise the image on the slicer.

The designs of the fore-optics, image slicers and spectrographs have been done independently, but they guarantee a perfect coupling between these subsystems by the definition of the interfaces shown in Table 3.

4 Image slicers as field re-formatters

In CUBES, the image slicers are field re-formatters, used to transform the rectangular field of view into a narrow long slit. They deliver the proposed spectral resolution without the need for Adaptive Optics in the UV and they reduce the sizes of the optical components of the spectrograph, thus reducing the overall dimensions and weight. We note that the CUBES science cases do not require a full IFU capability, so the sampling and on-sky fields of view of the slicers for both modes were optimised for single-object performance.

4.1 Optical design

A low complexity technical solution is adopted and the minimum number of surfaces has been considered to optimise throughput. The optical designs of the two image slicers are shown in Fig. 2. In both cases, the layouts are conceptually identical with different radius of curvature.

Each image slicer is composed of two arrays of six spherical slicer mirrors and six spherical camera mirrors of rectangular shape. For the HR image slicer each slice covers a field of 0.25arcsec width by 10arcsec length that leads to a size of 0.5mm x 20mm per slicer mirror. The size of the camera mirrors is 10mm width by 16.4mm length. The image slicer reformats the field generating the spectrograph entrance slit, whose dimensions are 88mm length by 0.19mm width. The slit is composed of the images of the six slices (slitlets) plus five gaps of 8.36mm each.

Since the magnification of both image slicers is the same, to provide different resolutions, the width of the slicers mirrors shall be thinner for the HR mode. The widths considered for these designs are 0.5mm (HR) and 2mm (LR) (see Tables 1 and 2). These widths do not represent any manufacturing challenge. For the LR image slicer, a field of view of 6arcsec by 10arcsec, corresponding to a linear size of 12mm x 20mm, is decomposed into six slices of 1arcsec width by 10arcsec length.

Table 3 Defined interfaces for the coupling fore-optics – image slicer and image slicer – spectrograph

Fore-optics – Image slicer	
Entrance pupil position (Fore-optics exit pupil)	1160.39mm before the slicer mirrors
Plate scale at slicer position	0.5arcsec/mm
Image slicer – Spectrograph	
Slit length specification	≤90mm
Slit width	0.19mm (HR), 0.77mm (LR)
Exit pupil position	3000mm from slitlets

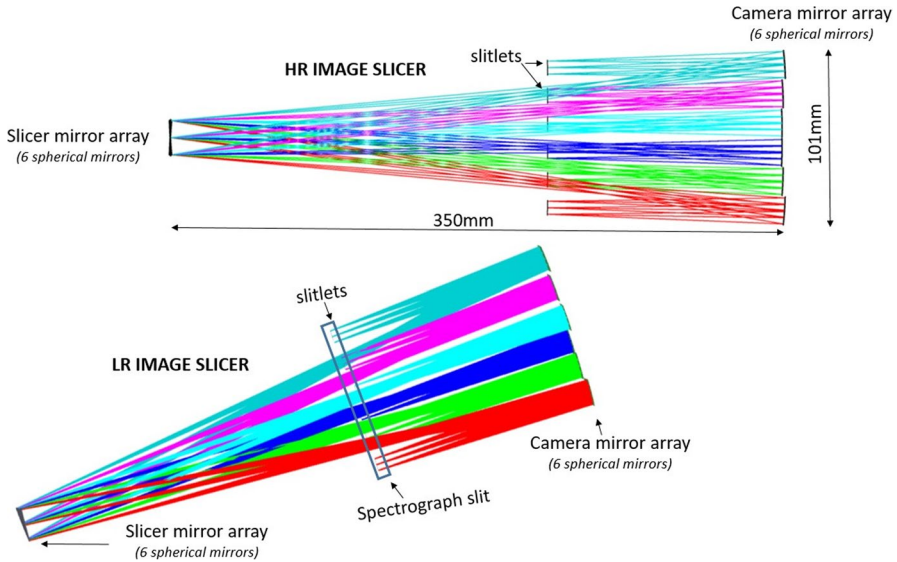


Fig. 2 Optical design of the HR and LR image slicers (top and bottom, respectively). In both cases the layout is composed of six spherical slicer mirrors and six spherical camera mirrors. An intermediate pupil image is located in between the two arrays and the exit pupil is placed at the spectrograph diffraction grating, where the six pupil images, associated to the six slices in which the entrance field of view was divided, are overlapped into a common pupil

The size of each slicer mirror is 2mm × 20mm. The size of the camera mirrors is 12mm width by 16.4mm length. The length of the HR and LR image slicers is approximately 350mm and they both produce a magnification of 0.383. These numbers are summarised in Table 4. The sizes for both resolution modes are shown in Fig. 3. There is an offset between the (parallel) input and output optical axes along the Y axis of 20mm.

Each image slicer will be contained within an independent housing. The two housings will be implemented on a motorised linear stage, giving the user the option

Table 4 Technical characteristics of the image slicer components

	HR	LR
Number of slicer mirrors	6	6
Curvature of slicer mirrors	Spherical	Spherical
Size of slicer mirrors	0.5mm × 20mm	2mm × 20mm
Number of camera mirrors	6	6
Size of camera mirrors	10mm × 16.4mm	12mm × 16.4mm
Size of generated slit	0.19mm × 88mm	0.77mm × 88mm
Number of slitlets	6	6
Separation between slitlets	8.36mm	8.36mm
Image slicer magnification	0.38	0.38

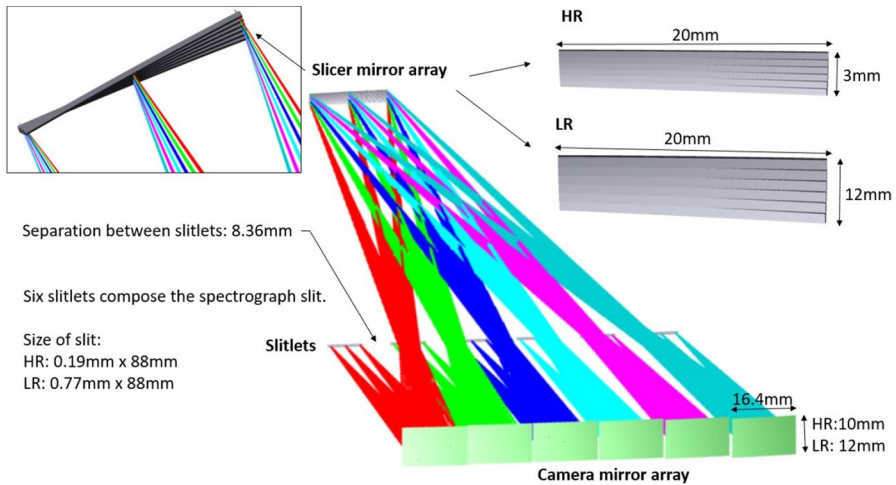


Fig. 3 Sizes of the components for the HR and LR images slicers. The slicer mirror array dimensions are 20mm length by 3mm width for HR, with six slicer mirrors of 0.5mm width. The dimensions for the LR slicer mirror array are 20mm by 12mm, with six slicer mirrors of 2mm width each. For both layouts the separation between slitlets is 8.36mm. Six slitlets and five separation gaps between them compose the spectrograph slit, whose dimensions are 0.19mm by 88mm for HR and 0.77mm by 88mm for LR

to select the resolution mode. The components of each image slicer are: slicer mirror array, camera mirror array, field/slit mask at the output slit position defining the spectrograph entrance slit and, optionally, a pupil mask at the intermediate pupil position to avoid potential stray light.

4.2 Analysis of aberrations

The spot diagrams at the output slit position for the HR and LR image slicers are shown in Figs. 4 and 5, respectively. Each column represents a slitlet, defined by seven field points and represented in a different colour according to the legend on the right. The circle is the Airy disk, which represents the diffraction limit. In these figures, the Airy radius is 7.089microns. The box in which the spot diagram for each field is represented has 50microns side.

The configurations associated with the central slices are 1 and 6. In this case the optical quality is limited by diffraction. The external slices correspond to configurations 3 and 4, which present the largest off-axis distances. The number of configurations is defined by the number of slices in which the entrance field of view is divided. This defines the number of mirrors in each array. Thus, each the rays associated to a slice of the field of view will have an optical path defined by the reflection in a slicer mirror and a camera mirror, generating a portion of the spectrograph slit or slitlet. These distributions within each image slicer are identified in Fig. 7 for the six configurations. The designs have been optimised to offer the best optical quality in the central slices, where most of the light will be contained. In both cases this is



Fig. 4 Optical quality of the HR image slicer evaluated at the output slit. Each column represents a slitlet defined by seven field points. The circle is the Airy disk, which defines the diffraction limit. the Airy radius is 7.089microns. The box in which the spot diagram for each field is represented has 50microns side. The configurations associated with the central slices are 1 and 6, with diffraction limited optical quality. The external slices correspond to configurations 3 and 4, which present the largest off-axis distances



Fig. 5 Optical quality of the LR image slicer evaluated at the output slit. Each column represents a slitlet defined by seven field points. The circle is the Airy disk, which defines the diffraction limit. the Airy radius is 7.089microns. The box in which the spot diagram for each field is represented has 50microns side. The configurations associated with the central slices are 1 and 6, with diffraction limited optical quality. The external slices correspond to configurations 3 and 4, which present the largest off-axis distances

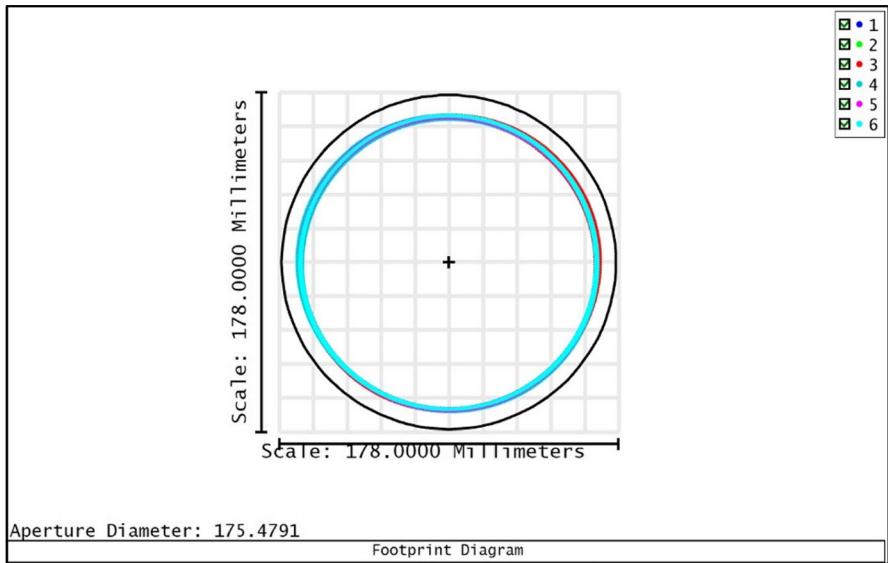


Fig. 6 Overlapped exit pupils at 3000mm from the slitlets. This is the diffraction grating position, where a common pupil is reconstructed after slicing the field of view

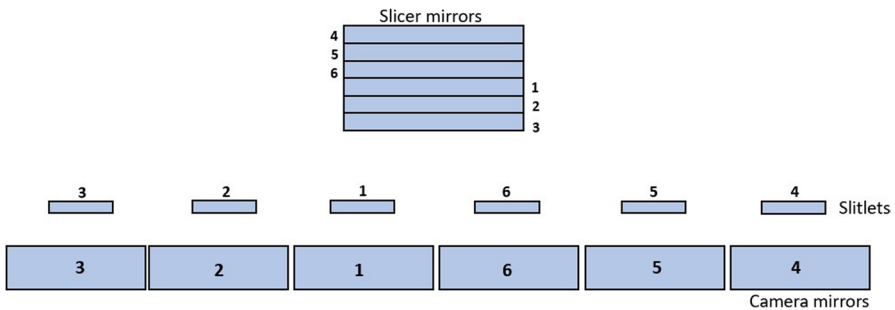


Fig. 7 Distribution of configurations for each component of the image slicer

diffraction limited. For the most external configurations (3 and 4) the main aberration is spherical, as expected due to the use of spherical mirrors. Although this could be improved using off-axis parabolic mirrors, spheres were initially selected to reduce complexity and costs. There is also a very small contribution of coma, field curvature and astigmatism.

Despite the optical quality of the image slicer being mostly diffraction limited, the fore-optics, located before the image slicer, produce some aberrations which ultimately deteriorate the optical performance at the slit-mask position. As a consequence, the image of the slices (slitlets) will be slightly wider than their nominal size, which implies a vignetting at the slit mask apertures. The slitlet apertures cannot be enlarged because these define the spectrograph slit aperture and thus the

resolution. The percentage of vignetting per slitlet was evaluated in Zemax using Geometric Image Analysis and considering the contribution of the telescope, fore-optics and image slicer. The smallest vignetting is expected for the central configurations (1, 6) in both resolution cases and the largest values for the external configurations (3, 4) and particularly for HR mode in which the slitlets are thinner. This is what is observed in the results. For the HR mode, the percentage of vignetting for the central configurations is $\approx 0.7\%$, $\approx 2\%$ for the middle configurations and a maximum of 3.6% for the external ones. For the LR mode, the vignetting is $\approx 0.2\%$ for the central configurations, $\approx 0.8\%$ for the middle ones and $\approx 1.6\%$ for the external configurations.

4.3 Exit pupil

Once the slicer mirror array has split the field into different slices, instead of an only pupil image, a pupil per slice is had. However, the tilt angles of the different components of the image slicer control the exit pupils orientations, which enables their overlapping in order to reconstruct the pupil. This is shown in the footprint diagram of Fig. 6, where the pupil for each configuration is represented as a ring in a different colour according to the legend on the top right. Meeting the interfaces with the spectrograph, the exit pupils for the six configurations are overlapped on a plane at 3000mm from the slitlet mask, where the spectrograph diffraction grating is located.

4.4 Slit distribution

Different slit distributions have been evaluated: staggered versus aligned and curved versus straight. The use of the same radius of curvature for all camera mirrors was investigated. This leads to a curved slit, curved field mask and a deterioration of the optical quality. To optimise the optical quality of the image slicer and spectrograph, different radii for each slicer mirror and each camera mirror are considered, providing a straight output slit generated by aligning the six slitlets associated to the images of the different slices of the field of view. In between slitlets there is a gap of 8.36mm. This separation is required to overlap all six pupil images on the diffraction grating (as shown in Fig. 6) and it also will avoid potential cross-talk through the slitlet apertures in the field mask. For the HR mode, the image slicer generates a slit of 88mm length by 0.19mm width. For the LR mode, the dimensions of the slit are 88mm length by 0.77mm width, meeting the interface defined in Table 3.

5 Critical parameters and manufacturing challenges

Although the presented designs are still at a conceptual level, the main critical parameters and potential manufacturing challenges have been taken into account. In the next project phases, the sensitivity and tolerance analysis will reveal more information to be discussed with the manufacturer. At this stage, those with a

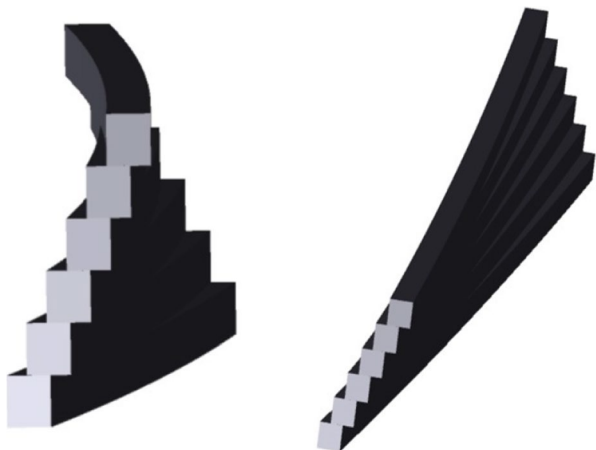
direct impact in the optical design were considered, such as the distribution and orientation of the components.

The distribution of the mirrors of each array in an image slicer, meaning the correspondence between a slice of the field (slicer mirror), camera mirror and image of that slice (slitlet), is very important to reduce angles of incidence and minimise aberrations. These designs have been optimised for the performance in the central slices, in which most of the light of a point source target will be contained. The distribution adopted, which is the same for both designs, is shown in Fig. 7, where all components denoted with the same number correspond to the same configuration and thus, to the same slice of the field of view. Within the slicer mirror array, the tilt angles are defined along the same direction to facilitate manufacturing, metrology and minimise potential shadows between adjacent slicer mirrors. This distribution is presented in Fig. 8, showing two views of the same array. Similar distributions are had for LR and HR.

Another important point to be considered is which substrate and coating will offer the best performance for the required spectral range. In order to reduce potential stray light, glass slicers have been considered since polishing will offer significantly better surface roughness than the results achievable on metal. The materials considered for the substrate are Zerodur or Fused Silica, both offering similar performance. Although the stray light analysis will be done during the next project phases, values for the surface roughness the order of 1nm RMS or lower are expected based on previous instruments.

At the CUBES wavelengths, the reflectivity using metallic coatings for the image slicer has been found to be about 90% per surface. With dielectric coatings it is possible to achieve 95% per surface, with a goal of 97%. It has been confirmed by the manufacturer based on their previous experience, that this dielectric coating will not produce any deformation on the slicer mirrors. For each image slicer, the slicer and camera mirrors will be integrated on a baseplate made of the same material as that for the image slicer components. This will avoid changes due to thermal effects.

Fig. 8 Two different views of the slicer mirror array showing the slicer mirror distribution where the tilt angles are defined along the same direction. Similar distribution has been adopted for HR and LR



6 Conclusions

Two image slicers are proposed for CUBES to offer two spectral resolution modes with $R \geq 20,000$ for high resolution and $R \geq 5,000$ for low resolution, facilitating observations for a wide variety of science cases within the 300 and 405nm spectral range. The addition of this subsystem presents these advantages:

- The use of image slicers as field re-formatters increases the spectral resolving power of the instrument and reduces the size of the spectrograph optics. This minimises the overall volume and weight, thus, enabling the spectrograph to be deployed at the Cassegrain focus within mass limits, with good spectral stability and low slit losses.
- The image slicers reformat a rectangular field of view of 3mm x 20mm (1.5arcsec by 10arcsec) into a slit of 0.19mm x 88mm for the HR mode and a field of view of 12mm x 20mm (6arcsec by 10arcsec) into a slit of 0.77mm x 88mm for the LR mode, enabling the choice of resolving power without the need for grating and/or other exchange mechanisms within the spectrograph.

Conceptually, the layout of both image slicers is the same, with different technical parameters for each resolution mode (like size and radius of curvature). The designs present low technical complexity and only two optical surfaces, with a total throughput of $\geq 90\%$. The mirrors in the image slicers will be manufactured in glass to reduce scattering at these UV wavelengths and with a dielectric coating to maximise efficiency.

The widths of the slicer mirrors are 0.5mm (HR) and 2mm (LR). The proposed solutions meet the required specifications and interfaces, provide an optical quality at the diffraction limit for the central configurations and are within current manufacturing capabilities.

Acknowledgements Sources of funding acknowledged are: A.C., K.O.B. and S.M. acknowledge the support received from the Science and Technology Facilities Council (STFC) UK (grant numbers ST/V00252X/1 and ST/V002597/1 at Durham University). W.S./LSW is grateful to the support from German BMBF under grant 05A20VHA.

Declarations

Conflicts of interest The authors declare that they have no conflict of interest.

Open Access This article is licensed under a Creative Commons Attribution 4.0 International License, which permits use, sharing, adaptation, distribution and reproduction in any medium or format, as long as you give appropriate credit to the original author(s) and the source, provide a link to the Creative Commons licence, and indicate if changes were made. The images or other third party material in this article are included in the article's Creative Commons licence, unless indicated otherwise in a credit line to the material. If material is not included in the article's Creative Commons licence and your intended use is not permitted by statutory regulation or exceeds the permitted use, you will need to obtain permission directly from the copyright holder. To view a copy of this licence, visit <http://creativecommons.org/licenses/by/4.0/>.

References

1. Evans, C.J., Barbury, B., Castilho, B., Smiljanic, R., Melendez, J., Japelj, J., Cristiani, S., Snodgrass, C., Bonifacio, P., Puech, M., Quirrenbach, A.: Revisiting the science case for near-UV spectroscopy with the VLT. *Proc. SPIE* **10702**(107022E), 10 (2018)
2. Ernandes, H., Evans, C.J., Barbury, B., Castilho, B., Cescutti, G., Christlieb, N., Cristiani, S., Di Marcantonio, P., Hansen, C., Quirrenbach, A., Smiljanic, R.: Stellar astrophysics in the near-UV with VLT-CUBES. *Proc. SPIE* 11447, *Ground-based and Airborne Instrumentation for Astronomy VIII*, 1144760 (2020)
3. Smiljanic, R., da Silva, A.R., Giribaldi, R.E.: Detecting weak beryllium lines with CUBES, ExA, [arXiv:2203.16158](https://arxiv.org/abs/2203.16158), in press as part of the Special Issue (2022)
4. Giribaldi, R.E., Smiljanic, R.: Beryllium abundances in turn-off stars of globular clusters with the CUBES spectrograph, ExA, [arXiv:2203.15604](https://arxiv.org/abs/2203.15604), in press as part of the Special Issue (2022)
5. Ernandes, H., Barbury, B., Castilho, B., et al.: Simulated observations of heavy elements with CUBES, ExA, [arXiv:2203.15693](https://arxiv.org/abs/2203.15693), in press as part of the Special Issue (2022)
6. Opitom, C., Snodgrass, C., La Forgia, F., et al.: Cometary Science with CUBES, ExA, [arXiv:2203.15579](https://arxiv.org/abs/2203.15579), in press as part of the Special Issue (2022)
7. D’Odorico, V.: Portraying the missing baryonic mass at the cosmic noon: the contribution of CUBES, ExA, (2022)
8. Zanutta, A., Atkinson, D., Baldini, V. et al. CUBES Phase-A design overview, ExA, (2022)
9. Dekker, H., D’Odorico, S., Kaufer, A., Delabre, B., Kotzlowski, H.: Design, construction, and performance of UVES, the echelle spectrograph for the UT2 Kueyen Telescope at the ESO Paranal Observatory. *Proc. SPIE* **4008**, 534–545 (2000)
10. Joel Vernet, H., Dekker, S., D’Odorico, L., Kaper, P., Kjaergaard, F., Hammer, S., Randich, F., Zerbi, P.M., Groot, J., Hjorth, I., Guinouard, R., Navarro, T., Adolfse, P.W., Albers, J.-P., Amans, J.J., Andersen, M.I., Andersen, P., Binetruy, P., Bristow, R., Castillo, F., Chemla, L., Christensen, P., Conconi, R., Conzelmann, J., Dam, V., De Caprio, A., De Ugarte Postigo, B., Delabre, P., Di Marcantonio, M., Downing, E., Elswijk, G., Finger, G., Fischer, H., Flores, P., Francois, P., Goldoni, L., Guglielmi, R., Haigron, H., Hanenburg, I., Hendriks, M., Horrobin, D., Horville, N.C., Jessen, F., Kerber, L., Kern, M., Kiekebusch, P., Kleszcz, J., Klougart, J., Kragt, H.H., Larsen, J.-L., Lizon, C., Lucuix, V., Mainieri, R., Manuputy, C., Martayan, E., Mason, R., Mazzoleni, N., Michaelsen, A., Modigliani, S., Moehler, P., Møller, A., Nørup Sørensen, P., Nørregaard, C., Peroux, F., Patat, E., Pena, J., Pragt, C., Reinero, F., Riga, M., Riva, R., Roelfsema, F., Royer, G., Sacco, P., Santin, T., Schoenmaker, P., Spano, E., Sweers, R., Ter Horst, M., Tintori, N., Tromp, P., van Dael, H., van der Vliet, L., Venema, M., Vidali, J., Vinther, P., Vola, R., Winters, D., Wistisen, G., Wulterkens, A.: Zacchei, X-shooter, the new wide band intermediate resolution spectrograph at the ESO Very Large Telescope. *Astron. Astrophys.* **536A**, 105 (2011)

Publisher’s note Springer Nature remains neutral with regard to jurisdictional claims in published maps and institutional affiliations.